BIOCHEMISTRY
including biophysical chemistry & molecular biology
Article

Biochemistry **2009,** *48,* 9641–9649 9641
DOI: 10.1021/bi900879a

Reaction Mechanism of *cis*-3-Chloroacrylic Acid Dehalogenase: A Theoretical Study†

Robin Sevastik,‡ Christian P. Whitman,*,§ and Fahmi Himo*,‡

‡*Department of Organic Chemistry, Arrhenius Laboratory, Stockholm University, SE-106 91 Stockholm, Sweden, and* §*Division of Medicinal Chemistry, College of Pharmacy, University of Texas, Austin, Texas 78712*

Received May 25, 2009; Revised Manuscript Received August 17, 2009

ABSTRACT: The reaction mechanism of *cis*-3-chloroacrylic acid dehalogenase (*cis*-CaaD) is studied using the B3LYP density functional theory method. This enzyme catalyzes the hydrolytic dehalogenation of *cis*-3-chloroacrylic acid to yield malonate semialdehyde and HCl. The uncatalyzed reaction is first considered, and excellent agreement is found between the calculated barrier and the measured rate constant. The enzymatic reaction is then studied with an active site model consisting of 159 atoms. The results suggest an alternative mechanism for *cis*-CaaD catalysis and different roles for some active site residues in this mechanism.

cis-3-Chloroacrylic acid dehalogenase (*cis*-CaaD) is a bacterial enzyme that catalyzes the hydrolytic dehalogenation of *cis*-3-chloroacrylic acid to produce malonate semialdehyde and HCl (Scheme 1) (*1*−*3*). *cis*-CaaD is part of a degradation pathway in the soil bacterium *Pseudomonas pavonaceae* allowing the bacteria to utilize 1,3-dichloropropene, a pesticide that is degraded to *cis*-3-chloroacrylic acid, as a source of carbon and energy (*4*).

cis-CaaD is a trimer composed of three identical monomers with 149 amino acids per monomer (*5*). It belongs to the tautomerase superfamily and shares sequence similarity with 4-oxalocrotonate tautomerase (4-OT) and *trans*-3-chloroacrylic acid dehalogenase (CaaD) (*6*, *7*). The latter enzyme catalyzes the same reaction as *cis*-CaaD but utilizes the *trans* substrate. All of the enzymes characterized thus far in the tautomerase superfamily have a catalytic terminal proline residue (Pro-1). In 4-OT, Pro-1 has a pK_a value of ∼6.4 and is proposed to act as a base, abstracting a proton from the substrate (*8*). In *cis*-CaaD, Pro-1 could act as a catalytic base to activate a water molecule for attack or it could function as a catalytic acid and provide a proton at C2 of the substrate to complete the conjugate addition of water. The pK_a of Pro-1 in CaaD has been determined to be ∼9.2 by direct NMR titration (*9*). In *cis*-CaaD, a direct NMR titration has not been performed. However, a pH−rate profile implicates a group in catalysis in the free enzyme with a pK_a of ∼9.3 (*10*). These results point toward Pro-1 being cationic in *cis*-CaaD, suggesting Pro-1 is not a catalytic base, but an acid.

All three enzymes have at least two arginine groups in the active site (Arg-70 and Arg-73 in *cis*-CaaD) that interact with the substrate's C1 carboxylate group. In *cis*-CaaD, the role of the arginine groups could be to draw electron density away from C3, facilitating the addition of water. Both CaaD and *cis*-CaaD have a glutamate residue in the active site (Glu-114 in *cis*-CaaD), which could be a potential base for activating the water molecule. An additional residue, His-28, is located near the two arginines in *cis*-CaaD. His-28 may assist in positioning the substrate and/or polarizing it via an interaction with the C1 carboxylate group.

†This work was supported by The Swedish Research Council (F.H.) and National Institutes of Health Grant GM-65324 (C.P.W.).

*To whom correspondence should be addressed. C.P.W.: telephone, +1-512-471-6198; fax, +1-512-232-2606; e-mail, whitman@mail.utexas.edu. F.H.: telephone, +46-8-161094; fax, +46-8-154908; e-mail, himo@organ.su.se.

On the basis of experimental studies (*11*−*13*), a general mechanism for the *cis*-CaaD reaction has been proposed (Scheme 2). A base (i.e., Glu-114) in the active site activates a water molecule for attack at the C3 position of the substrate to form a tetrahedral intermediate. The tetrahedral intermediate then collapses to an enol intermediate (path a), which is followed by ketonization to give the final product. Alternatively, the tetrahedral intermediate picks up a proton at C2 (path b) followed by collapse and release of HCl and product.

The barriers for the uncatalyzed and CaaD-catalyzed reaction of the dehalogenation of *trans*-3-chloroacrylic acid have been determined experimentally to be ∼33.3 and 16.6 kcal/mol, respectively (*14*). CaaD thereby achieves an $\sim 10^{12}$-fold rate enhancement. A similar rate enhancement for *cis*-CaaD can be assumed in view of the similarities between the two substrates and enzymes.

In this study, we investigate the reaction mechanism of *cis*-CaaD using the B3LYP density functional theory method (*15*−*18*). A relatively large model of the active site (159 atoms) is constructed, and the two different mechanistic hypotheses are considered (Scheme 2). In addition, the impact of the protonation state of Pro-1 on the mechanism is considered. This approach has been proven to be very useful in the study of a wide variety of enzymatic reactions (*19*−*33*). In particular, we have previously used the same approach to investigate the reaction mechanism of 4-oxalocrotonate tautomerase (*28*).

COMPUTATIONAL DETAILS

All geometries and energies presented in this study are computed using the B3LYP (*15*−*18*) density functional theory method as implemented in the Gaussian03 program package (*34*). Geometry optimizations were performed using the 6-31G(d,p) basis set. On the basis of these geometries, single-point calculations with the larger 6-311+G(2d,2p) basis set were conducted to produce more accurate energies. Solvation energies were added as single-point calculations using the conductor-like solvation model CPCM (*35*, *36*) at the B3LYP/6-31G(d,p) level. In this model, a cavity around the system is surrounded by a polarizable dielectric continuum. For the uncatalyzed solution reaction (see Model of the Uncatalyzed Reaction), a dielectric constant of 80 is used to model the water surrounding. To model the enzyme

Published on Web 09/02/2009

Scheme 1: Reaction Catalyzed by *cis*-3-Chloroacrylic Acid Dehalogenase

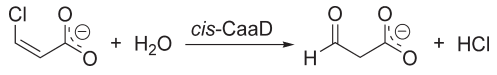

Scheme 2: Proposed Reaction Mechanisms for *cis*-3-Chloroacrylic Acid Dehalogenase

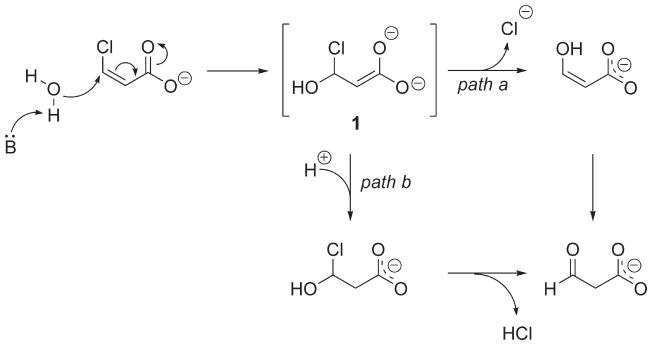

surrounding, an ε of 4 is used. However, since this value is rather arbitrary, the results using an ε of 80 are also reported here to give an idea about the sensitivity of the results. In the active site model, some centers were kept fixed to their X-ray positions in the geometry optimization. The size of the model (i.e., 159 atoms) prohibited the calculation of frequencies and thus the determination of the zero-point vibrational energies and the entropy effects. The energies reported here correspond thus to enthalpies. Another problem related to the size of the model is the multiple-minimum problem. To avoid the case in which the stationary points lie in different local minima, which can lead to unreliable relative energies, we have by careful visual inspection done our best to confirm that the parts that do not directly participate in the reaction are in the same local minima throughout the reaction.

RESULTS AND DISCUSSION

Model of the Uncatalyzed Reaction. Wolfenden and coworkers measured the uncatalyzed rate for the hydrolytic dehalogenation of the *trans* isomer to be 2.2×10^{-12} s^{-1}, which corresponds to a rate-limiting barrier of 33.3 kcal/mol (*14*). The uncatalyzed rate for the *cis* isomer is likely to be comparable.

We devised a small model consisting of the *cis*-3-chloroacrylic acid substrate and two water molecules to study the uncatalyzed reaction. The optimized stationary points are shown in Figure 1, and the calculated energies are displayed in Figure 2.

In the first step, one water molecule attacks at C3, while the second water shuttles the proton from the nucleophilic water to the carboxylate moiety of the substrate. At the transition state, the critical O−C distance is 2.05 Å and the C−Cl distance is 1.81 Å (only slightly longer than the distance of 1.77 Å calculated for the reactant species). It turns out that the nucleophilic attack and the displacement of the chloride ion take place in a single step. Numerous attempts were made to locate a tetrahedral intermediate (e.g., **1** in Scheme 2) without success. The barrier is calculated to be 30.2 kcal/mol, and the reaction step was found to be exothermic by as much as 27.3 kcal/mol. Addition of solvation in the form of the polarizable continuum model (PCM) with a dielectric constant ε of 80 had very little effect on these energies (Figure 2). The barrier increased slightly to 31.8 kcal/mol, and the reaction energy was slightly increased, to −25.7 kcal/mol. The calculated barrier agrees very well with the experimental value of 33.3 kcal/mol. This indicates that the model, despite its small size, captures the important features of the reaction.

The second step is a 1,3-keto−enol tautomerization step to give malonate semialdehyde. This step was also studied with help of two water molecules [**4** (Figure 1)]. In the gas phase, this reaction step is slightly exothermic (−1.4 kcal/mol), while upon addition of solvation (ε = 80), it is slightly endothermic (1.9 kcal/mol). We have located the transition state [**5** (Figure 1)], and the barrier was calculated to be 16.8 kcal/mol. When solvation was added, the barrier became 19.9 kcal/mol.

The addition of more water molecules to the model did not change the energies significantly. For example, the barrier for the first step was calculated to be 34.0 kcal/mol (ε = 80) when using five water molecules in the model.

Two conclusions can be drawn from the results of our study of the nonenzymatic reaction. First, the rate-limiting barrier for the transformation is found for the first step, which is a nucleophilic attack and chloride release. The enzymatic barrier has been estimated to be 16.6 kcal/mol (*14*), which means that *cis*-CaaD has to lower the barrier of the first step by more than 16 kcal/mol, assuming it uses a similar reaction mechanism. The second conclusion is that since the barrier of the second step is relatively low, it is possible that this step could be nonenzymatic, taking place outside the enzyme. This suggests that *cis*-CaaD may catalyze only the first step of the reaction.

Model of the Enzymatic Reaction. A model of the *cis*-CaaD active site was built on the basis of the native crystal structure [Protein Data Bank (PDB) entry 2FLZ (*5*)]. The model consists of parts of the following residues (as shown schematically in Figure 3): Pro-1, Glu-114, Tyr-103′, Leu-119, Arg-70, His-69, Arg-73, His-28, and Thr-34 (where the prime indicates that the residue comes from an adjacent monomer). The substrate was not present in the native crystal structure and had therefore to be superimposed on the basis of the crystal structure of *cis*-CaaD inactivated by (*R*)-oxirane-2-carboxylate (PDB entry 2FLT). Inactivation results from the covalent attachment of (*R*)-2-hydroxypropanoate on Pro-1 (*5*). Also, the water molecule was added manually in the vicinity of the potential bases Pro-1 and Glu-114. The model thus consists of 159 atoms, and the total charge is 0. To maintain the overall active site structure and to avoid artificial movements of various groups, we locked certain atoms in their crystallographic positions. These are typically the positions at which the truncation is made. These positions are indicated by asterisks in the figures below.

In the optimized reactant structure, the two arginines (Arg-70 and Arg-73) and the histidine (His-28) bind the carboxylate moiety of the substrate, thereby positioning it in the active site. The water molecule is in good position to attack C3 of the substrate, with an O−C3 distance of 3.66 Å. The water is hydrogen-bonded to Pro-1 (2.43 Å) and Glu-114 (2.32 Å), indicating that both of these groups are possible bases that can activate the water. It should be noted that the optimal pH for the reaction is ∼9.0 (*8*). If the pK_a of Pro-1 is ∼9.2, then a significant percentage of the enzyme has a neutral Pro-1 (∼40%) and a cationic Pro-1 (∼60%).

We optimized the transition state for the nucleophilic attack of water (Figure 3C). As in the case of the uncatalyzed reaction, this step turns out to be coupled to the release of the chloride ion. At the TS, the O−C3 distance is 1.76 Å and the C3−Cl distance increased from 1.75 Å in the reactant to 1.80 Å. The water hydrogen bonds to Pro-1 and Glu-114 are also significantly shorter, 1.62 and 1.60 Å, respectively.

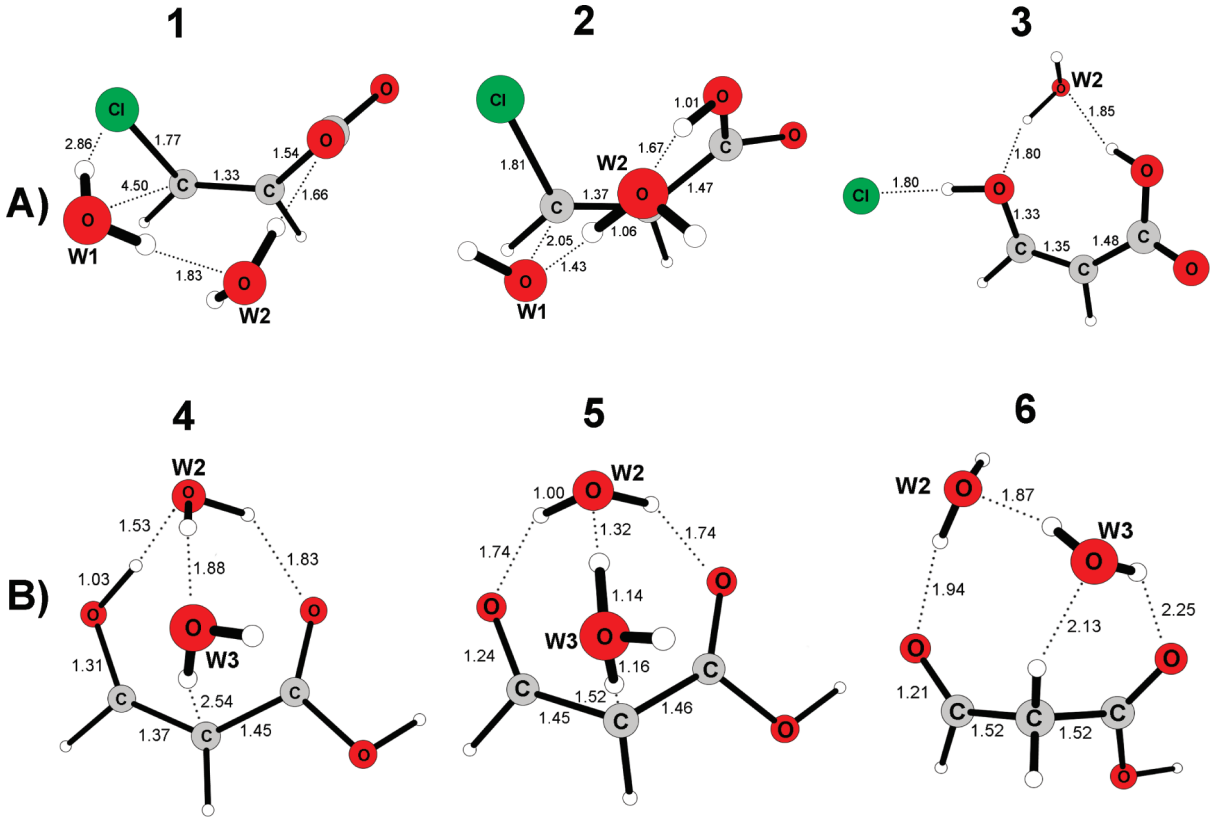

FIGURE 1: Optimized stationary points for the first dehalogenation step (A) and the second tautomerization step (B) of the nonenzymatic reaction: (1) reactant structure, (2) transition state, (3) enol intermediate, (4) enol intermediate, (5) transition state, and (6) keto product.

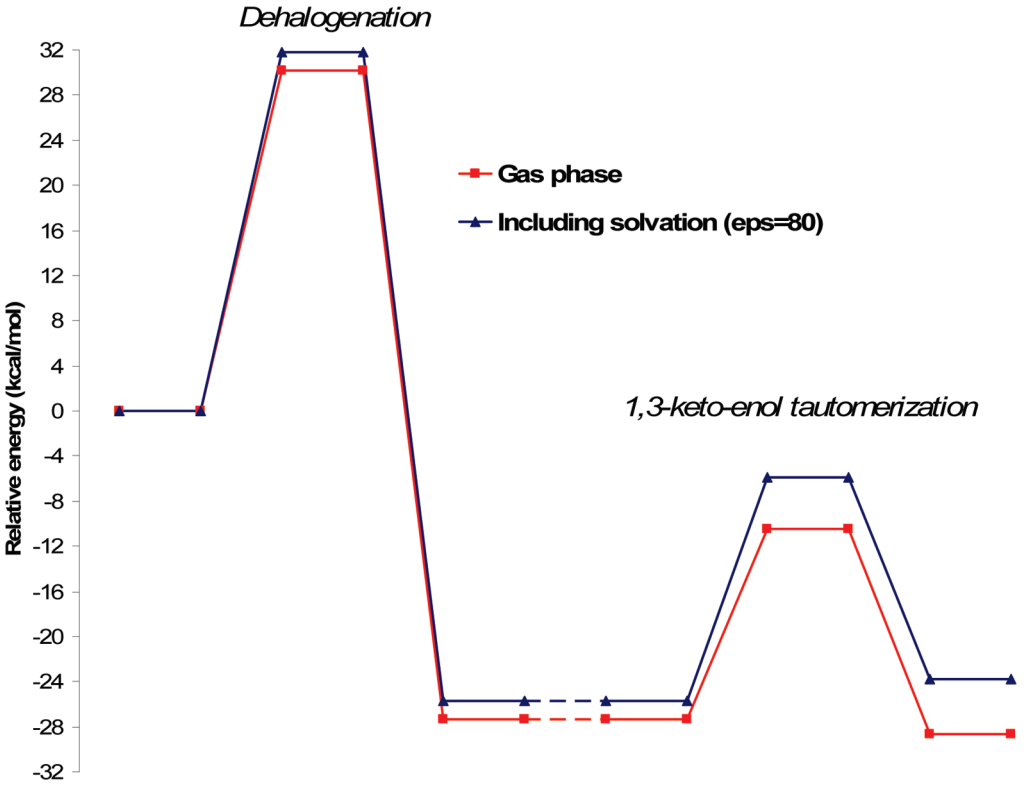

FIGURE 2: Calculated potential energy curve for the uncatalyzed reaction.

In the resulting enol intermediate, the chloride is totally released. It turns out that the proton of the water is transferred to Pro-1, which in turn transferred its proton to Glu-114. Glu-114 is thus the catalytic base that activates the water molecule, and one of the functions of Pro-1 could be to shuttle the proton.

The calculated barrier for this step is 22.3 kcal/mol, which upon inclusion of solvation effects decreases slightly to 21.9 and

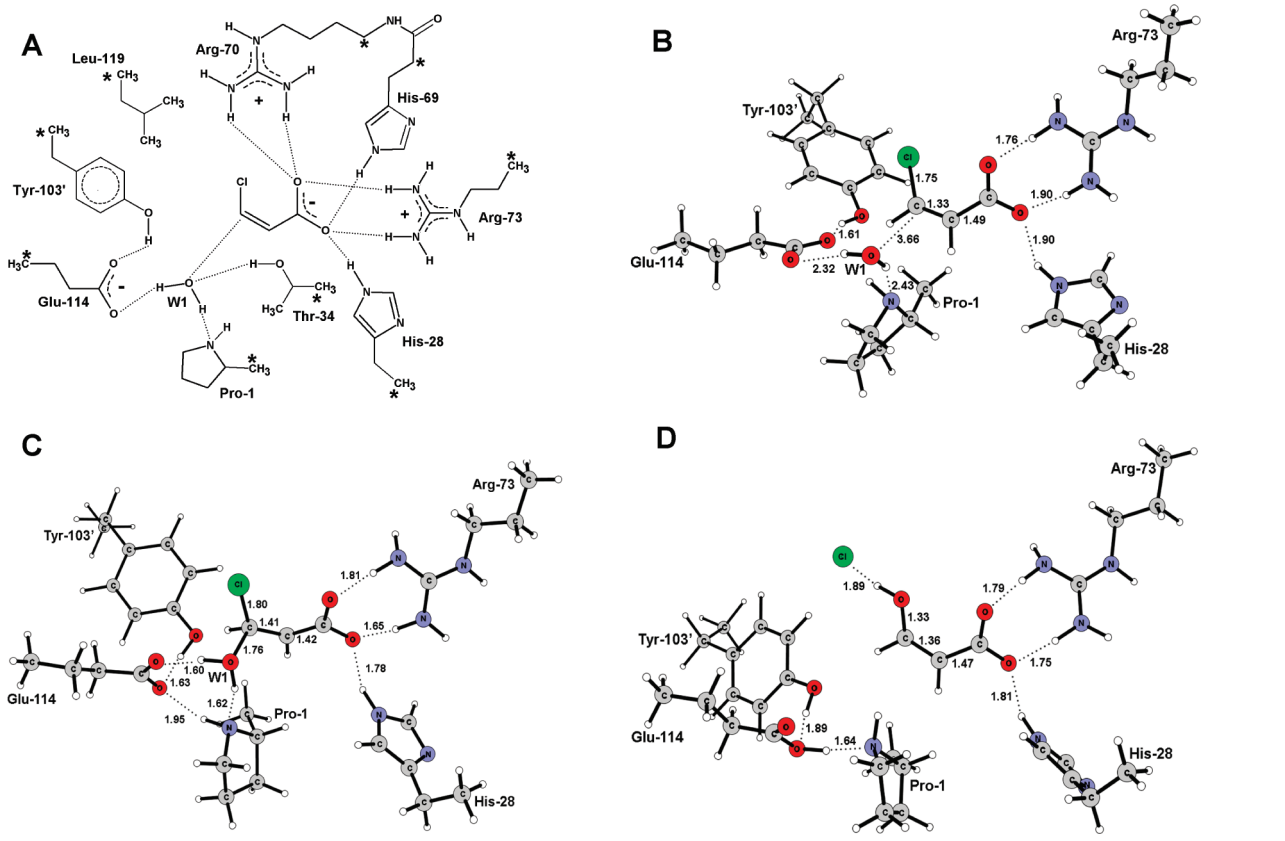

FIGURE 3: Optimized geometries of the enzymatic model of *cis*-CaaD with a neutral Pro-1. (A) Schematic drawing of the model. (B) Reactant geometry. (C) Transition state geometry. (D) Product geometry. Optimized distances are given in angstroms. Asterisks indicate centers that are fixed to their crystallographic positions during geometry optimization, as discussed in the text. For the sake of clarity, several groups were omitted from the ball-and-stick structures (B−D).

21.7 kcal/mol, using dielectric constants (ε) of 4 and 80, respectively. As in the nonenzymatic case, the reaction step is highly exothermic, by 33.6, 36.9, and 38.3 kcal/mol, without solvation and with solvation using ε values of 4 and 80, respectively.

In this kind of dehalogenation reaction where an ion is released in the active site, the electrostatic interactions with the enzyme surroundings are expected to contribute significantly to the energetics. However, the fact that the solvation effects are quite small (< 1 kcal/mol for the barrier) indicates that the chosen model is adequate for describing this kind of reaction. This is an important result that is in line with previous experience from enzyme modeling where we have observed that the solvation effects saturate at a model size similar to the one used in this study (*28*, *32*).

Once the enol intermediate has formed in the *cis*-CaaD enzyme, a ketonization reaction follows to generate the final product. This could take place outside the enzyme. The barrier for this is calculated to be 19.9 kcal/mol, as discussed above.

To model the tautomerization step at the active site, we removed the chloride ion from the model and reoptimized the enol intermediate (Figure 4A). We note the existence of a hydrogen bond network that connects the substrate enol to Pro-1, which is in perfect position to protonate C2 of the substrate. This network involves the Tyr-103′ and Glu-114 residues.

We tried to locate a transition state in which the proton is transferred concertedly through this chain, but without success. Instead, the enzymatic tautomerization was found to proceed in a stepwise fashion. First, a proton was transferred from Glu-114 to Pro-1. This step has a very small barrier of 0.6 kcal/mol and is slightly exothermic (by 2.2 kcal/mol, values referring to an ε of 4). Next, a concerted proton transfer from the substrate enol to Tyr-103′ coupled with a proton transfer from Tyr-103′ to Glu-114 takes place. The barrier for this step is also quite low (6.2 kcal/mol), and it is slightly endothermic (2.0 kcal/mol). Finally, the cationic Pro-1 can now deliver the proton to the C2 position of the substrate, thereby completing the reaction. This step has a significant barrier of 13.6 kcal/mol, which, when added to the endothermicity of the previous step, becomes 15.6 kcal/mol. The overall enzymatic ketonization reaction is thus endothermic by 8.2 kcal/mol. The optimized structures are shown in Figure 4, and the calculated energies of the entire *cis*-CaaD reaction are summarized in Figure 5.

Hence, according to this model, the difference between the enzymatic and nonenzymatic keto−enol tautomerization step is quite small (ca. 4 kcal/mol) and within the margin of error, which allows the possibility that the reaction takes place outside the active site.

Alternative Water Binding. Since it is unknown how the substrate and the water molecule bind relative to each other in the active site, we examined an alternative binding mode in which the water is positioned on the other face of the substrate, i.e., far from Pro-1 (see Figure 6). The water now forms a hydrogen bond to the Tyr-103′ residue instead of Pro-1 and Glu-114 in the former case (see above).

Also for this model, we optimized the transition state for nucleophilic attack of water and found that attack and release of the chloride ion occur in a single step. The catalytic base is the same, Glu-114. However, Tyr-103′ takes the role of the Pro-1 residue in shuttling the proton to the base.

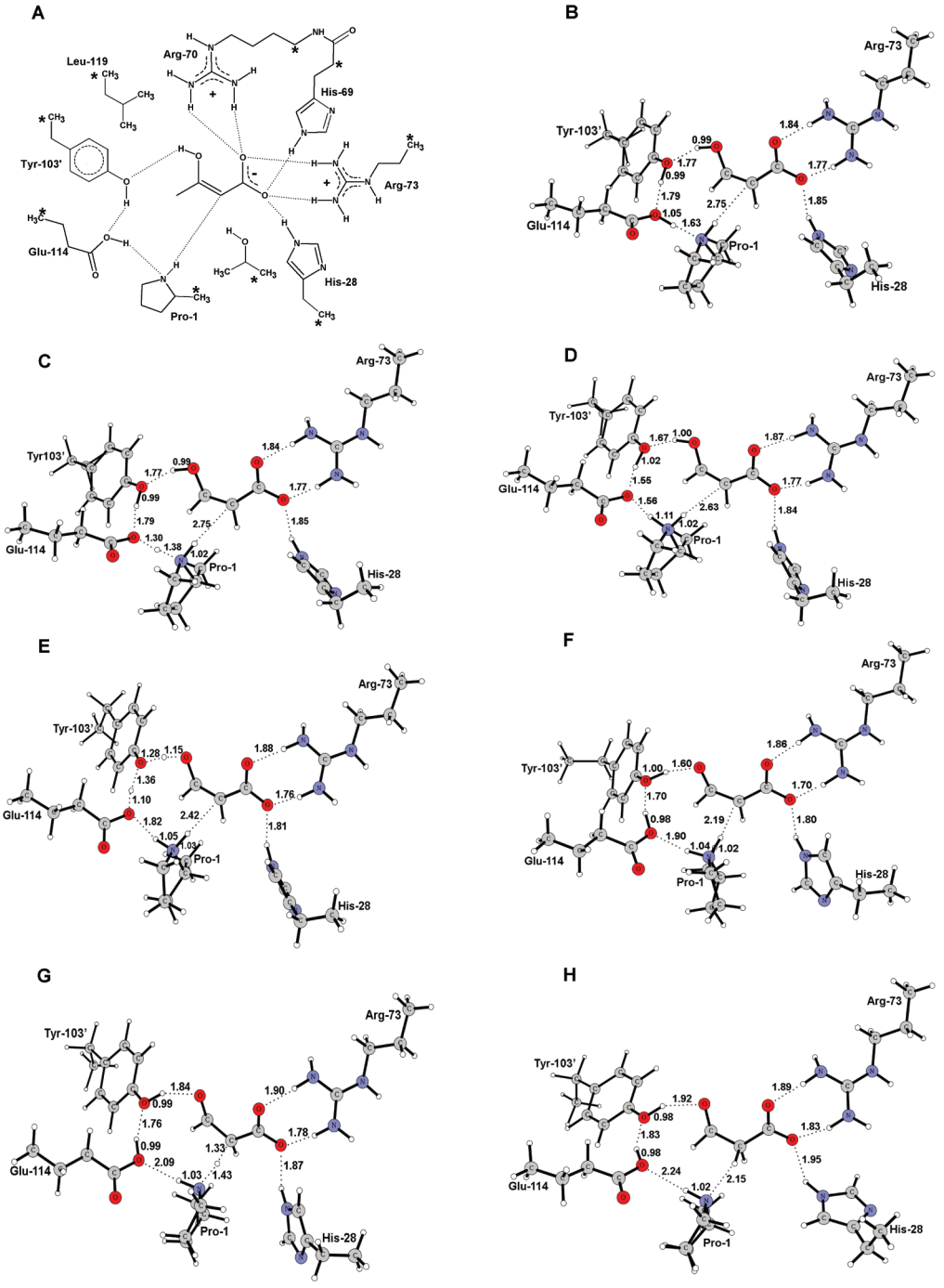

FIGURE 4: Optimized stationary points for a proposed enzymatic keto−enol reaction. (A) Schematic drawing of the model. (B) Enol intermediate. (C) TS for the transfer of a proton from Glu-114 to Pro-1. (D) Resulting intermediate with a cationic Pro-1. (E) TS for the coupled transfers of protons from substrate to Tyr-103′ and from Tyr-103′ to Glu-114. (F) Resulting enolate intermediate. (G) TS for transfer of a proton from Pro-1 to substrate. (H) Final product. For the sake of clarity, several groups were omitted in the ball-and-stick structures (B−H).

The calculated barrier for this scenario is 20.6 kcal/mol, which upon inclusion of solvation increases to 26.4 and 28.5 kcal/mol using ε values of 4 and 80, respectively. These values are significantly higher than those calculated for the other binding mode, making this scenario less likely.

Cationic Pro-1. In the calculations presented above, Pro-1 was modeled in the neutral form. However, as noted above, a significant fraction (~60%) is cationic, and it has been proposed that Pro-1 functions as a general acid (*9*). Therefore, we constructed a model of the active site in which Pro-1 was in the cationic form. The model has a total of 160 atoms and a total charge of +1 (Figure 7).

In the reactant structure, the water is in a good position to attack the substrate, with an O−C3 distance of 3.56 Å, and the water is hydrogen bonded to the Glu-114 residue.

For this model, we have optimized the transition state for the nucleophilic attack, which is coupled with the dehalogenation of the substrate. In this model, Glu-114 acts directly as the catalytic base, activating the nucleophilic water molecule. In the transition state, the critical O−C3 distance is 1.77 Å and the C3−Cl distance is 1.81 Å.

The calculated barrier is 27.6 kcal/mol, which increases to 31.7 and 33.1 kcal/mol with ε values of 4 and 80, respectively. These values are ~10 kcal/mol higher than that calculated

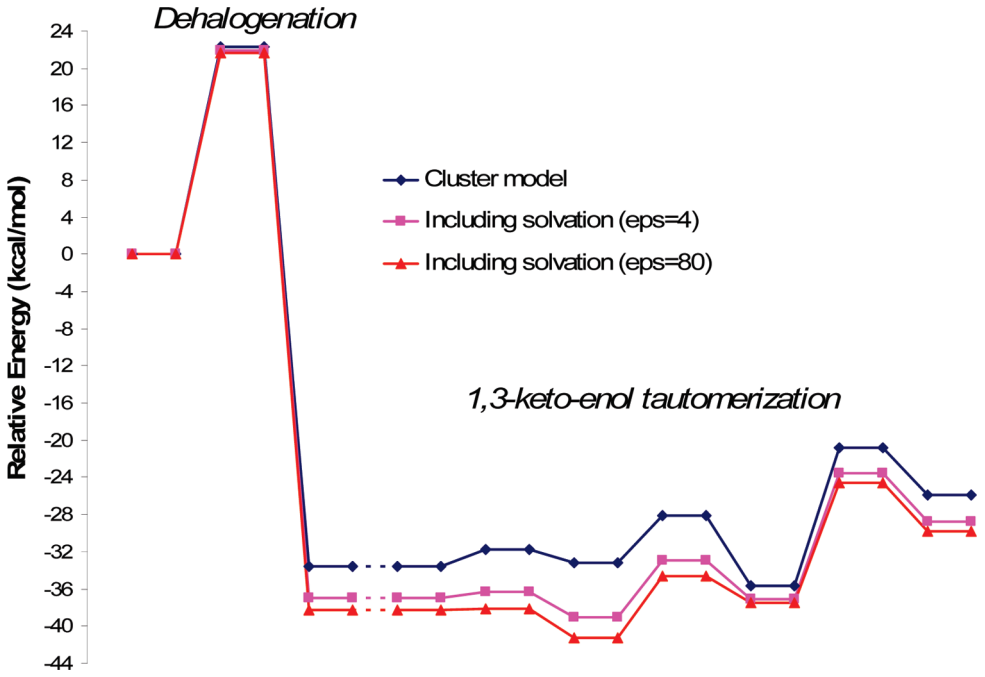

FIGURE 5: Calculated potential energy curve for the *cis*-CaaD reaction. The ε of 4 is the standard dielectric constant used to model protein surroundings, and the ε of 80 corresponds to a water solution.

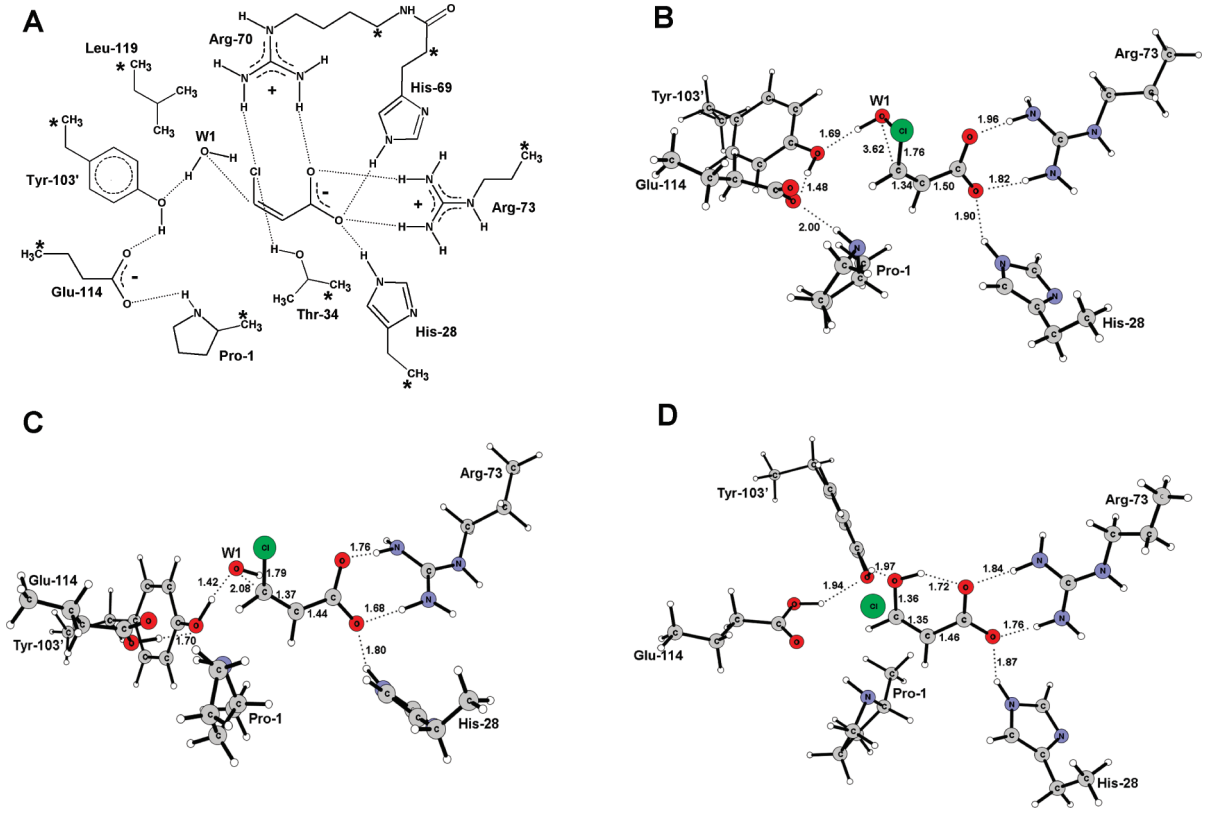

FIGURE 6: Optimized geometries of the enzymatic model of *cis*-CaaD with a neutral Pro-1 and an alternative position of the water molecule. (A) Schematic drawing of the model. (B) Reactant geometry. (C) Transition state geometry. (D) Product geometry. Optimized distances are given in angstroms. Asterisks indicate centers that are fixed to their crystallographic positions during geometry optimization. In the ball-and-stick structures (B−D), several groups were omitted for the sake of clarity.

for the neutral proline case, arguing strongly against a cationic Pro-1.

One striking result here is the reaction energy of this step. With a neutral proline, the reaction step is highly exothermic (36.9 kcal/mol using an ε of 4). However, with a cationic proline, this value is only −3.2 kcal/mol, despite the fact that the catalytic base is the same Glu-114. This can be understood if one considers the Glu-Pro dyad as one unit. This unit is negatively charged when Pro-1 is neutral (Glu-COO^--Pro-NH) and neutral when Pro-1 is cationic (Glu-COO^--Pro-NH_2^+ or alternatively Glu-COOH-Pro-NH). Thus, the proton affinity of this Glu-Pro unit is considerably different in the two cases. In the latter case, the Glu-Pro unit is a

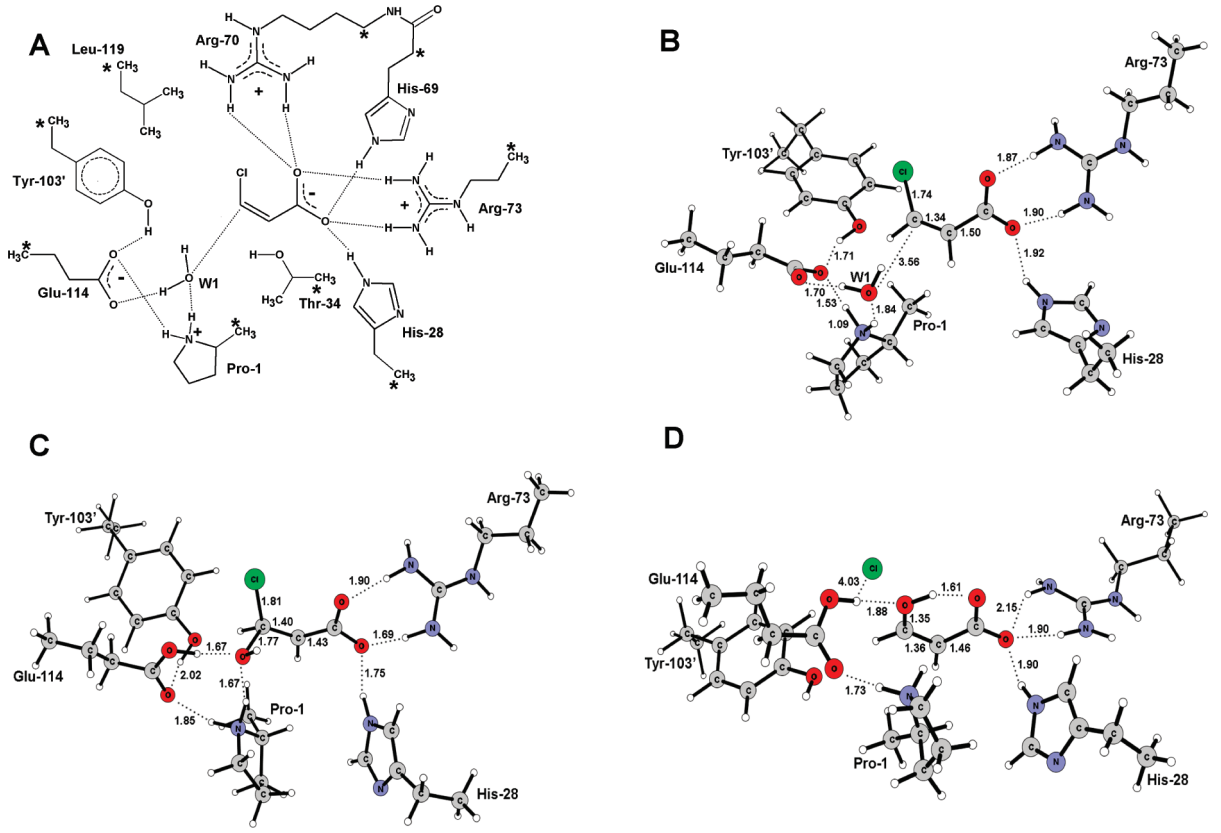

FIGURE 7: Optimized geometries of the enzymatic model of *cis*-CaaD with a cationic Pro-1. (A) Schematic drawing of the model. (B) Reactant geometry. (C) Transition state geometry. (D) Product geometry. Optimized distances are given in angstroms. Asterisks indicate centers that are fixed to their crystallographic positions during geometry optimization. In the ball-and-stick structures (B−D), several groups were omitted for the sake of clarity.

Scheme 3: Main Elements of the *cis*-CaaD Reaction Mechanism Suggested from the Calculations

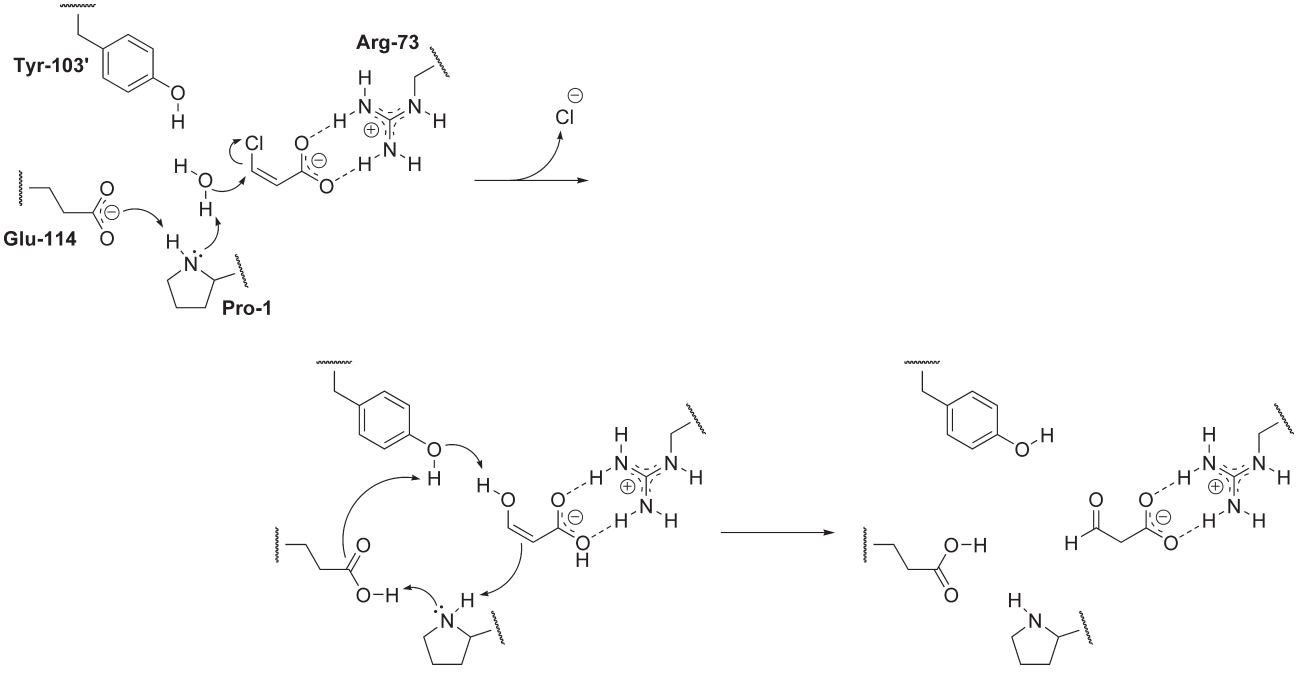

worse proton acceptor and thus a worse base, which explains the large difference in the calculated exothermicities.

Mechanistic Implications. In the current working hypothesis for the *cis*-CaaD mechanism, Tyr-103 and Glu-114 work together (in some fashion) to activate a water molecule for attack at C3 of the substrate (*2*, *5*, *10*). In this scenario, His-28 and the pair of arginine residues (Arg-70 and Arg-73) bind and activate the substrate via the C1 carboxylate group. This interaction polarizes the substrate such that a partial positive charge develops at C3, which facilitates the attack of water at C3. Pro-1, functioning as a catalytic acid, adds a proton to C2 to complete the addition of water. The finding that the reaction is more energetically favorable

Table 1: Summary of Calculated Energies (kilocalories per mole) for the Dehalogenation Step in the Active Site Model

	neutral Pro-1		alternative water binding		cationic Pro-1	
	barrier	reaction energy	barrier	reaction energy	barrier	reaction energy
cluster model	22.3	−33.6	20.6	−32.4	27.6	−0.2
$\varepsilon = 4$	21.9	−36.9	26.4	−31.6	31.7	−3.2
$\varepsilon = 80$	21.7	−38.3	28.5	−31.4	33.1	−4.6

when a neutral proline is involved (rather than a cationic proline) is obviously at odds with the currently proposed mechanism, particularly with the roles of Pro-1, Tyr-103, and Glu-114.

The *cis*-CaaD mechanism was formulated on the basis of sequence similarities and mechanistic parallels with CaaD, coupled with crystallographic observations of the unliganded *cis*-CaaD enzyme and the enzyme inactivated by (*R*)-oxirane-2-carboxylate (*2*, *5*, *10*). A sequence alignment with CaaD first identified the four common groups (i.e., Pro-1, Arg-70, Arg-73, and Glu-114) (*2*). Mutagenesis analysis confirmed the importance of these groups but suggested a subtle mechanistic difference: the Gln-114 mutant retained a significant amount of activity, whereas the α-Gln-52 mutant of CaaD had no activity. The crystallographic observations identified two more residues (His-28 and Tyr-103) and pointed to a more complex mechanism for *cis*-CaaD (*5*). A very recent pre-steady state kinetic analysis of the *cis*-CaaD reaction suggested that a short loop closes down on the active site upon substrate binding (B. A. Robertson, G. K. Schroeder, Z. Jin, K. A. Johnson, and C. P. Whitman, 2009, unpublished results). The loop is not present in CaaD, indicating yet another mechanistic difference. Thus, as new details emerge about the *cis*-CaaD mechanism, it is becoming apparent that there may only be limited parallels between CaaD and *cis*-CaaD and some of the underlying assumptions used to formulate the *cis*-CaaD mechanism may not be entirely valid.

One assumption concerns the protonation state of the prolyl nitrogen in *cis*-CaaD. The pK_a of the prolyl nitrogen (*β*-Pro-1) in CaaD has been determined to be 9.2 by direct titration using ^{15}N NMR spectroscopy (*9*). A direct titration of Pro-1 in *cis*-CaaD has not been conducted, but a pH−rate profile of the *cis*-CaaD reaction implicated an acid catalyst with a pK_a of 9.3 in the reaction (*12*). It is assumed that this pK_a value corresponds to that of Pro-1 (and that the acid catalyst is Pro-1) on the basis of the coincident pK_a values and the mechanistic parallels. The results of this study suggest that this assumption and the role of Pro-1 in the reaction should be examined in more detail.

A second assumption concerns the roles of Tyr-103 and Glu-114. The assigned roles for these residues are based on their positions in the crystal structures of the native and inactivated enzyme complex (along with the analogous role of α-Glu-52 in CaaD). It may be that the interactions of these two residues and their possible interactions with Pro-1 are more complex. One possible mechanism is shown in Scheme 3.

CONCLUSIONS

In this study, we investigated the reaction mechanism of *cis*-CaaD using density functional theory calculations and a large active site model.

First, a model of the uncatalyzed reaction was studied, and excellent agreement was found with the experimental rate. The calculations indicate that the nucleophilic attack of water at C2 and release of the chloride ion happen in one step.

The enzymatic reaction mechanism suggested from the calculations is summarized in Scheme 3. Similar to the water reaction, the enzymatic nucleophilic attack and dehalogenation step are calculated to happen in one step. Glu-114 acts as the catalytic base to activate the nucleophilic water molecule. However, Pro-1 might shuttle the proton from water to the base. Mutagenic analysis shows that replacement of Pro-1 with an alanine reduced activity to an undetectable rate, whereas changing Glu-114 to a glutamine decreased activity by only 6−8-fold (as assessed by k_{cat}/K_m) (*2*). These results are consistent with the calculated mechanism since it is conceivable that removal of the proline shuttle makes it more difficult to activate the water, while when the Glu-114 base is removed, Pro-1 itself can act as the catalytic base in a fashion analogous to its function in the related enzyme 4-oxalocrotonate tautomerase.

Next, a ketonization reaction takes place to complete the reaction. The calculations indicate that it is possible for the active site Tyr-Glu-Pro triad to shuttle the proton from the oxygen to the carbon (in a stepwise fashion). The calculated barrier for this is 15.6 kcal/mol compared to the barrier of 19.9 kcal/mol calculated for the nonenzymatic counterpart.

The calculated rate-limiting barrier of ca. 22 kcal/mol is somewhat overestimated compared to the experimentally determined barrier for the closely related CaaD [16.6 kcal/mol (*14*)]. Several sources of error are envisioned. As always in quantum chemical studies, the computational method (in this case, the DFT/B3LYP functional and the employed basis sets) cannot be ruled out as a possible source of error. Another error could be introduced by the size of the model used in the investigations. Inclusion of more active site groups might lead to a lower reaction barrier. Also, locking truncation atoms can lead to a model that is somewhat rigid, which causes the barriers to be higher. Finally, the crystal structure used for the modeling is that of the irreversibly inactivated enzyme. It is not known how accurately this structure reflects substrate binding and turnover. These inaccuracies coupled with the obtained resolution of the structure can easily translate into errors in the calculations.

In this study, we also considered the possibility of the Pro-1 being cationic. However, the barrier was found to be much higher, arguing against this option. Also, an alternative binding mode of the nucleophilic water relative to the substrate was considered, in which the Tyr-103′ residue would act as the proton shuttle instead of Pro-1. However, the barrier becomes significantly higher, rendering this possibility less likely. The calculated energies for the various scenarios are summarized in Table 1.

REFERENCES

1. Poelarends, G. J., Saunier, R., and Janssen, D. B. (2001) *trans*-3-Chloroacrylic acid dehalogenase from *Pseudomonas pavonaceae* 170 shares structural and mechanistic similarities with 4-oxalocrotonate tautomerase. *J. Bacteriol. 183*, 4269–4277.
2. Poelarends, G. J., Serrano, H., Person, M. D., Johnson, W. H. Jr., Murzin, A. G., and Whitman, C. P. (2004) Cloning, expression, and characterization of a *cis*-3-chloroacrylic acid dehalogenase: Insights into the mechanistic, structural, and evolutionary relationship

between isomer-specific 3-chloroacrylic acid dehalogenases. *Biochemistry 43*, 759–772.
3. Wang, S. C., Person, M. D., Johnson, W. H. Jr., and Whitman, C. P. (2003) Reactions of *trans*-3-chloroacrylic acid dehalogenase with acetylene substrates: Consequences of and evidence for a hydration reaction. *Biochemistry 42*, 8762–8773.
4. Poelarends, G. J., Wilkens, M., Larkin, M. J., van Elsas, J. D., and Janssen, D. B. (1998) Degradation of 1,3-dichloropropene by *Pseudomonas cichorii* 170. *Appl. Environ. Microbiol. 64*, 2931–2936.
5. de Jong, R. M., Bazzaco, P., Poelarends, G. J., Johnson, W. H. Jr., Kim, Y. J., Burks, E. A., Serrano, H., Thunnissen, A.-M. W. H., Whitman, C. P., and Dijkstra, B. W. (2007) Crystal structures of native and inactivated *cis*-3-chloroacrylic acid dehalogenase: Structural basis for substrate specificity and inactivation by (*R*)-oxirane-2-carboxylate. *J. Biol. Chem. 282*, 2440–2449.
6. Whitman, C. P. (2002) The 4-oxalocrotonate tautomerase family of enzymes: How nature makes new enzymes using a β-α-β structural motif. *Arch. Biochem. Biophys. 402*, 1–13.
7. Poelarends, G. J., and Whitman, C. P. (2004) Evolution of enzymatic activity in the tautomerase superfamily: Mechanistic and structural studies of the 1,3-dichloropropene catabolic enzymes. *Bioorg. Chem. 32*, 376–392.
8. Stivers, J. T., Abeygunawardana, C., Mildvan, A. S., Hajipour, G., and Whitman, C. P. (1996) 4-Oxalocrotonate tautomerase: pH dependence of catalysis and pK_a values of active site residues. *Biochemistry 35*, 814–823.
9. Azurmendi, H. F., Wang, S. C., Massiah, M. A., Poelarends, G. J., Whitman, C. P., and Mildvan, A. S. (2004) The roles of active-site residues in the catalytic mechanism of *trans*-3-chloroacrylic acid dehalogenase: A kinetic, NMR, and mutational analysis. *Biochemistry 43*, 4082–4091.
10. Poelerands, G. J., Serrano, H., Johnson, W. H. Jr., and Whitman, C. P. (2004) Stereospecific alkylation of *cis*-3-chloroacrylic acid dehalogenase by (*R*)-oxirane-2-carboxylate: Analysis and mechanistic implications. *Biochemistry 43*, 7187–7196.
11. de Jong, R. M., Brugman, W., Poelarends, G. J., Whitman, C. P., and Dijkstra, B. W. (2004) The X-ray structure of *trans*-3-chloroacrylic acid dehalogenase reveals a novel hydration mechanism in the tautomerase superfamily. *J. Biol. Chem. 279*, 11546–11552.
12. Poelarends, G. J., Johnson, W. H. Jr., Serrano, H., and Whitman, C. P. (2007) Phenylpyruvate tautomerase activity of *trans*-3-chloroacrylic acid dehalogenase: Evidence for an enol intermediate in the dehalogenase reaction? *Biochemistry 46*, 9596–9604.
13. Poelarends, G. J., Almrud, J. J., Serrano, H., Darty, J. E., Johnson, W. H. Jr., Hackert, M. L., and Whitman, C. P. (2006) Evolution of enzymatic activity in the tautomerase superfamily: Mechanistic and structural consequences of the L8R mutation in 4-oxalocrotonate tautomerase. *Biochemistry 45*, 7700–7708.
14. Horvat, C. M., and Wolfenden, R. V. (2005) A persistent pesticide residue and the unusual catalytic proficiency of a dehalogenating enzyme. *Proc. Natl. Acad. Sci. U.S.A. 102*, 16199–16202.
15. Becke, A. D. (1988) Density-functional exchange-energy approximation with correct asymptotic-behavior. *Phys. Rev. A 38*, 3098–3100.
16. Becke, A. D. (1992) Density-functional thermochemistry 1. The effect of the exchange-only gradient correction. *J. Chem. Phys. 96*, 2155–2160.
17. Becke, A. D. (1992) Density-functional thermochemistry 2. The effect of the Perdew-Wang generalized-gradient correlation correction. *J. Chem. Phys. 97*, 9173–9177.
18. Becke, A. D. (1993) Density-functional thermochemistry 3. The role of exact exchange. *J. Chem. Phys. 98*, 5648–5652.
19. Himo, F., and Siegbahn, P. E. M. (2003) Quantum chemical studies of radical-containing enzymes. *Chem. Rev. 103*, 2421–2456.
20. Himo, F. (2006) Quantum chemical modeling of enzyme active sites and reaction mechanisms. *Theor. Chem. Acc. 116*, 232–240.
21. Siegbahn, P. E. M., and Himo, F. (2009) Recent developments of the quantum chemical cluster approach for modeling enzyme reactions *J. Biol. Inorg. Chem. 14*, 643–651.
22. Hopmann, K. H., Hallberg, B. M., and Himo, F. (2005) Catalytic mechanism of limonene epoxide hydrolase, a theoretical study. *J. Am. Chem. Soc. 127*, 14339–14347.
23. Velichkova, P., and Himo, F. (2005) Methyl transfer in glycine N-methyltransferase. A theoretical study. *J. Phys. Chem. B 109*, 8216–8219.
24. Himo, F., Guo, J.-D., Rinaldo-Matthis, A., and Nordlund, P. (2005) Reaction mechanism of deoxyribonucleotidase: A theoretical study. *J. Phys. Chem. B 109*, 20004–20008.
25. Hopmann, K. H., and Himo, F. (2006) Theoretical study of the full reaction mechanism of human soluble epoxide hydrolase. *Chem.—Eur. J. 12*, 6898–6909.
26. Velichkova, P., and Himo, F. (2006) Theoretical study of the methyl transfer in guanidinoacetate methyltransferase. *J. Phys. Chem. B 110*, 16–19.
27. Chen, S.-L., Fang, W.-H., and Himo, F. (2007) Theoretical study of the phosphotriesterase reaction mechanism. *J. Phys. Chem. B 111*, 1253–1255.
28. Sevastik, R., and Himo, F. (2007) Quantum chemical modeling of enzymatic reactions: The case of 4-oxalocrotonate tautomerase. *Bioorg. Chem. 35*, 444–457.
29. Chen, S.-L., Marino, T., Fang, W.-H., Russo, N., and Himo, F. (2008) Peptide hydrolysis by the binuclear zinc enzyme aminopeptidase from *Aeromonas proteolytica*: A density functional theory study. *J. Phys. Chem. B 112*, 2494–2500.
30. Liao, R.-Z., Yu, J.-G., Raushel, F. M., and Himo, F. (2008) Theoretical investigation of the reaction mechanism of the dinuclear zinc enzyme dihydroorotase. *Chem.—Eur. J. 14*, 4287–4292.
31. Hopmann, K. H., and Himo, F. (2008) Cyanolysis and azidolysis of epoxides by haloalcohol dehalogenase: Theoretical study of the reaction mechanism and origins of regioselectivity. *Biochemistry 47*, 4973–4982.
32. Hopmann, K. H., and Himo, F. (2008) Quantum chemical modeling of the dehalogenation reaction of haloalcohol dehalogenase. *J. Chem. Theory Comput. 4*, 1129–1137.
33. Liao, R.-Z., Yu, J.-G., and Himo, F. (2009) Reaction mechanism of the dinuclear zinc enzyme n-acyl-L-homoserine lactone hydrolase: a quantum chemical study. *Inorg. Chem. 48*, 1442–1448.
34. Frisch, M. J. (2004) Gaussian 03 , revision C.02, Gaussian, Inc., Wallingford, CT.
35. Barone, V., and Cossi, M. (1998) Quantum calculation of molecular energies and energy gradients in solution by a conductor solvent model. *J. Phys. Chem. A 102*, 1995–2001.
36. Cossi, M., Rega, N., Scalmani, G., and Barone, V. (2003) Energies, structures, and electronic properties of molecules in solution with the C-PCM solvation model. *J. Comput. Chem. 24*, 669–681.